DE GRUYTER

Rev. Adv. Mater. Sci. 2021; 60:15–24

Research Article

Silu Liu and Yonghao Zhao*

Mechanical properties, deformation and fracture mechanisms of bimodal Cu under tensile test

Abstract: Metals with a bimodal grain size distribution have been found to have both high strength and good ductility. However, the coordinated deformation mechanisms underneath the ultrafine-grains (UFGs) and coarse grains (CGs) still remain undiscovered yet. In present work, a bimodal Cu with 80% volume fraction of recrystallized micro-grains was prepared by the annealing of equal-channel angular pressing (ECAP) processed ultrafine grained Cu at 473 K for 40 min. The bimodal Cu has an optimal strength-ductility combination (yield strength of 220 MPa and ductility of 34%), a larger shear fracture angle of 83° and a larger area reduction of 78% compared with the as-ECAPed UFG Cu (yield strength of 410 MPa, ductility of 16%, shear fracture angle of 70°, area reduction of 69%). Grain refinement of recrystallized micro-grains and detwinning of annealing growth twins were observed in the fractured bimodal Cu tensile specimen. The underlying deformation mechanisms for grain refinement and detwinning were analyzed and discussed.

Keywords: Bimodal grain size distribution, UFG Cu, grain coarsening, detwinning

1 Introduction

Bulk ultrafine-grain (UFG) materials possess high strength but low ductility, which has evolved into a seemingly insurmountable obstacle for widespread technological applications of these new materials [1–8]. Recently, various strategies have been developed for improving the poor ductility of bulk UFG materials [1, 9], among which, in-troducing a bimodal or multi-modal grain size distribution has been found to be broadly applicable to many material systems [10–13]. These bimodal or multi-modal materials usually have a wide grain size distribution ranging from the UFG (*i.e.*, <500 nm) to the coarse-grain (CG, >1 μm) scales [14], and they can be prepared by annealing-induced secondary recrystallization of UFG materials [12] or via the consolidation of mixtures of multi-scale sized particles [13, 14]. Since large amount of published work has qualitatively verified that the introduction of bimodal microstructures can indeed improve the poor ductility of UFG materials [15–22], a question, of how the UFGs and CGs coordinate with each other to attain the high ductility, is naturally proposed.

Inspection of the published literature shows that there is only a limited number of reports on deformation and fracture mechanisms of bimodal metals and alloys [11, 12, 23–26]. A theory from the field of fracture mechanics was used to explain the good tensile ductility [11]. A crack is initiated at an internal flaw and propagates rapidly through the UFG region. The crack can be blunted by CGs because it must propagate along the appropriate slip system of the large grains. Wang *et al.* applied finite element modeling in combination with post-mortem transmission electron microscopy analysis [12]. They reported that during deformation, the CGs, which are embedded in the heterogeneous microstructure, experience multi-axial stress state conditions, consisting of triaxial strain components and large strain gradients. Strain-gradient plasticity theory [27] suggests that an excessively large number of geometrically necessary dislocations are required to accommodate the large strain gradients, thereby resulting in significant strain hardening and large uniform elongation. Moreover, Lee *et al.* [23] reported that the fracture surface of a bimodal Al-Mg alloy, containing 30% volume fraction of CGs prepared by cryomilling and subsequent power consolidation techniques, shows a mixed fracture mode: large shear lips with a flat central region. Scanning electron microscopy revealed that voids near the tensile fracture surfaces tend to initiate both in the UFG matrix as well as at the UFG and CG interfaces.

More recently, a back stress between UFG and CG regions based on dislocation piling-up model has been pro-

*Corresponding Author: Yonghao Zhao: Nano and Heterogeneous Materials Center, School of Materials Science and Engineering, Nanjing University of Science and Technology, Nanjing 210094, China; Email: yhzhao@njust.edu.cn
Silu Liu: Nano and Heterogeneous Materials Center, School of Materials Science and Engineering, Nanjing University of Science and Technology, Nanjing 210094, China

posed to explain the origins of high strain hardening and ductility of bimodal and heterogeneous Ti etc. metals [24–26, 28]. The abovementioned investigations in literatures revealed deformation of bimodal metals from viewpoints of mechanics, and fracture by numerical simulation and experiments. However, the coordinated deformation mechanisms underneath the UFGs and CGs from viewpoints of microstructural evolutions still remain unknown yet.

In this work, we first prepared UFG Cu by employing equal-channel angular pressing (ECAP) technique, and then prepared bimodal Cu by annealing the as-ECAPed UFG Cu at 473 K for 40 min. Finally, we systematically investigated microstructure evolution, deformation and fracture mechanisms of the bimodal Cu during tensile deformation. Compared with the UFG Cu, the bimodal Cu exhibited optimal strength-ductility combination. Electron backscattered diffraction (EBSD) post-mortem observation of the bimodal Cu after tension revealed grain refinement of the recrystallized CGs and detwinning of annealing growth twins, contributing to the high ductility of the bimodal Cu.

2 Materials and methods

In this work, high-purity UFG copper (99.99%) square bars were prepared by ECAP at ambient temperature by route Bc and 90° die angle for 16 passes [29, 30]. The as-ECAPed UFG Cu was then annealed at 473 K in silicone oil for 40 min to form bimodal structures with 80% volume fraction of recrystallized micro-grains.

Flat dog-bone tensile specimens with gauge dimensions of 10×1×2 mm were sectioned by electrical discharge machining (EDM). Uniaxial tensile tests were performed at room temperature on an Instron 8801 universal testing machine (UTM) with an initial quasi-static strain rate of 10^{-3} s^{-1}. The strain was measured by using a standard non-contacting video extensometer with a 100 mm field-of-view lens.

The grip sections of the tensile specimens were examined using transmission electron microscopy (TEM) at a Philips CM12 microscope operated at 100 kV and EBSD at a TSL OIM system on a Philips XL30 FEG SEM with step sizes of 50-100 nm. TEM specimens were prepared by first mechanically grinding the samples to a thickness of about 50–70 μm, then dimpling to a thickness of about 10 μm, and finally ion-milling to a thickness of electron transparency using a Gatan Precision Ion Milling System with an Ar+ accelerating voltage of 4 kV and a temperature below 308 K. The EBSD samples were first polished using a diamond lapping film (particle diameter 1 μm) and then electro-polished

in a solution of 66% H_3PO_4 and 34% H_2O at 2 V. The fracture surface and morphology was imaged by a FEI-XL30 SFEG SEM using a 25 kV beam.

3 Results

3.1 Microstructures of as-ECAPed UFG Cu and as-annealed bimodal Cu

Figure 1(a) and (b) present typical bright-field TEM images and the corresponding selected area electron diffraction (SAED) patterns (taken from an area with a diameter of 5.4 μm) of the as-ECAPed and annealed Cu samples, respectively. The as-ECAPed Cu sample was composed of equiaxed grains with sizes ranging from about 100 nm to 1 μm and an average size of about 300 nm. Moreover, two types of grains were observed: clean and dislocation free grains with sharp equilibrium boundaries (as indicated by white arrows) and dislocation decorated grains with wavy distorted boundaries (indicated by black arrows in the figure). The sharp equilibrium boundaries may have originated from relaxation, recovery or even recrystallization during the ECAP process. The wavy distorted boundaries are mainly sub-grain (dislocation cell) boundaries with low-angle misorientation and non-equilibrium boundaries [31], which contain a high density of extrinsic dislocations.

After annealing for 40 min, as shown in Figure 1(b), recrystallized micro-grains with sizes ranging from 1 to 3 μm dominated the sample. Annealing twins were frequently observed in these micro-grains, as highlighted by white arrows in Figure 1(b). To further confirm the microstructures of the bimodal Cu, we performed EBSD analysis, as shown in Figure 1(c). It is apparent that the UFG matrices were uniformly distributed within the recrystallized micro-grains and inter-connected so that the recrystallized micro-grain regions were separated into isolated regions. Quantitative calculation indicates that the volume fraction of the recrystallized macro-grains is about 80%.

Figure 1(d) shows local average misorientation map of the annealed Cu sample. This map calculated the average misorientation between every pixel and its surrounding pixels, and assigns the mean value to that pixel. The rainbow bar on top of Figure 1(d) is the reference code of color-misorientation, in which blue, green and red colors represent low (< 1°), medium (from 1° to 3°) and high (from 3° to 5°) misorientation. The blue (volume fraction 81%) and non-blue (volume fraction 19%, composed by green mainly and minor yellow) areas perfectly corresponded to the locations of recrystallized micro-grains and deformed
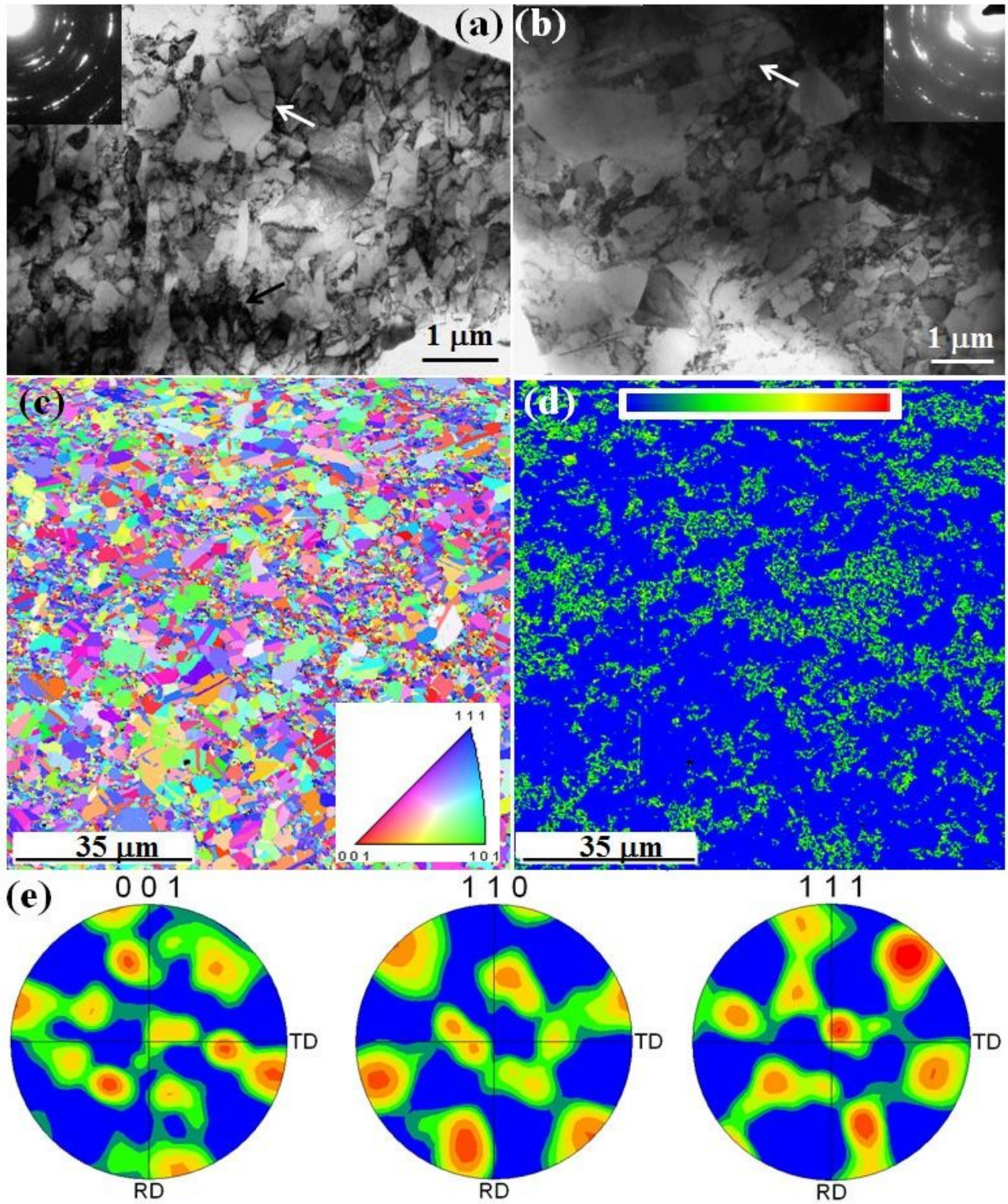
Figure 1: (a) Bright-field TEM image of the as-ECAPed UFG Cu. The inset is the corresponding selected area electron diffraction (SAED) patterns taken from an area with a diameter of 5.4 µm. (b) Bright-field TEM image of the annealed bimodal Cu. The inset is the corresponding SAED patterns taken from an area with a diameter of 5.4 µm. (c) EBSD orientation mapping of the bimodal Cu, the inset is IPF-Z coloring code; (d) the local average misorientation map of Figure 1(c), inset rainbow bar is the reference code of color-misorientation, in which blue, green and red colors represent low (< 1°), medium (from 1° to 3°) and high (from 3° to 5°) misorientation; (e) the pole figures of Figure 1(c).

UFGs as in Figure 1(c), respectively. The local average misorientation was less than $1°$ in the blue areas of Figure 1(d), which implied the free dislocation condition in the recrystallized grains of Figure 1(b). The non-blue areas with local average misorientation between $1°$ and $3°$ in Figure 1(d) confirmed the deformed UFGs with internal dislocation pile-ups and cells in Figure 1(b).

Figure 1(e) shows {001}, {110} and {111} pole figures in stereographic projection of the bimodal Cu. {110} and {111} pole figures were indicative of the shearing effect from ECAP and agreed well with textures evolved from the ECAP of 90 ° die-angle, route Bc and 16-pass in early reports [32, 33]. As stated in [31], texture evolution in ECAP is governed mainly by three factors: applied deformation, deformation mechanisms and initial textures. The applied deformation item matters about the facility parameters in ECAP, such as die angle, route and pass number. However, {001} pole figure exhibited deviated textures from the ideal ones [32, 33] in ECAP. The site and symmetry deviation of projected points in the {001} pole figure would be expected from the annealing process and following recrystallization.

3.2 Mechanical properties

The engineering stress-strain curves of as-ECAPed and annealed bimodal Cu samples are shown in Figure 2. It is apparent that the as-ECAPed Cu sample has a dominant post-necking elongation. This geometrical instability is the typical phenomenon of UFG metals processed by severe plastic deformation due to the lack of strain hardening and dislocation accumulation capability. As listed in Table 1, the as-ECAPed Cu sample has a 0.2% yield strength of 370 MPa, ultimate tensile strength of 410 MPa, an uniform elongation of 2% and an elongation to the failure of 16%. Annealing for 40 min decreased the yield strength of the Cu sample (220 MPa) by enhancing strain hardening and ductility (34%).

3.3 Fracture mechanisms

To understand the fracture mechanisms in the as-ECAPed and annealed Cu samples, we studied the fracture mode and morphology using the SEM. Sample as-ECAPed Cu
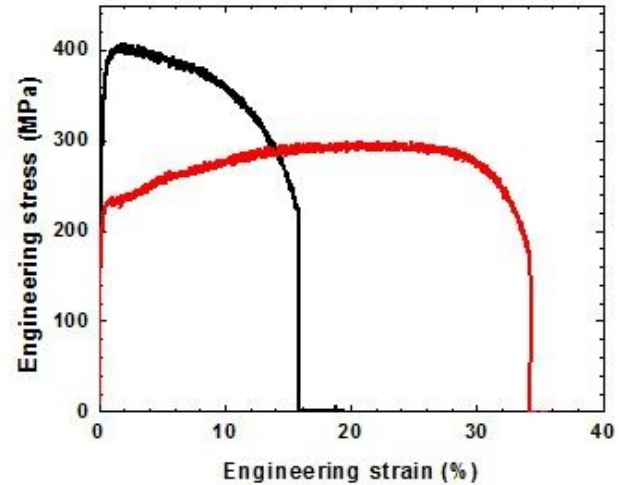
Figure 2: Tensile engineering stress-strain curves of as-ECAP (black) and bimodal Cu (red).

failed in a shear fracture mode with a shear fracture angle θ of about $70°$ [Figure 3(a)]. The shear fracture is attributable to the nanostructures which resulted in a decreased ratio of the average critical normal fracture stress to shear fracture stress [34]. Careful examination on the cross-sectional surface near the fracture edge in Figure 3(a) revealed some deformed micro-bands parallel to fracture edge [denoted by red arrow in Figure 3(b)]. Figure 3(c) and (d) shows SEM images of the fracture surfaces of samples as-ECAPed Cu. The fracture area reduction A is 69% and the dimples were slightly elongated with sizes ranging from about 5 to 20 μm due to void nucleation and subsequent coalescence via shear fracture.

The annealed bimodal Cu had a larger shear fracture angle of $83°$ as in Figure 3(e). The deformed micro-bands in horizontal direction were pointed by red arrow, while in Figure 3(f) elongated regions in vertical direction with a thickness smaller than 1 μm (pointed by green arrow) were the elongated recrystallized micro-grains as revealed by the following EBSD results. The fracture area reduction is 78% as in Figure 3(g) and two types of dimples were observed in Figure 3(h) and the zoom-in view of Figure 3(i): dominant deep micrometer-sized dimples and small amount of homogeneously distributed shallow sub-micrometer-sized dimples as pointed by blue arrows. This observation was

Table 1: A list of yield strength $\sigma_{0.2}$, ultimate tensile strength σ_{UTS}, uniform elongation ϵ_{ue}, elongation to failure ϵ_{ef}, area reduction A and shear fracture angle θ of the as-ECAPed Cu and annealed bimodal Cu.

Samples	$\sigma_{0.2}$, MPa	σ_{UTS}, MPa	ϵ_{ue}, %	ϵ_{ef}, %	A (%)	θ (°)
As-ECAPed Cu	370	410	2	16	69	70
Annealed Cu	220	297	18	34	78	83
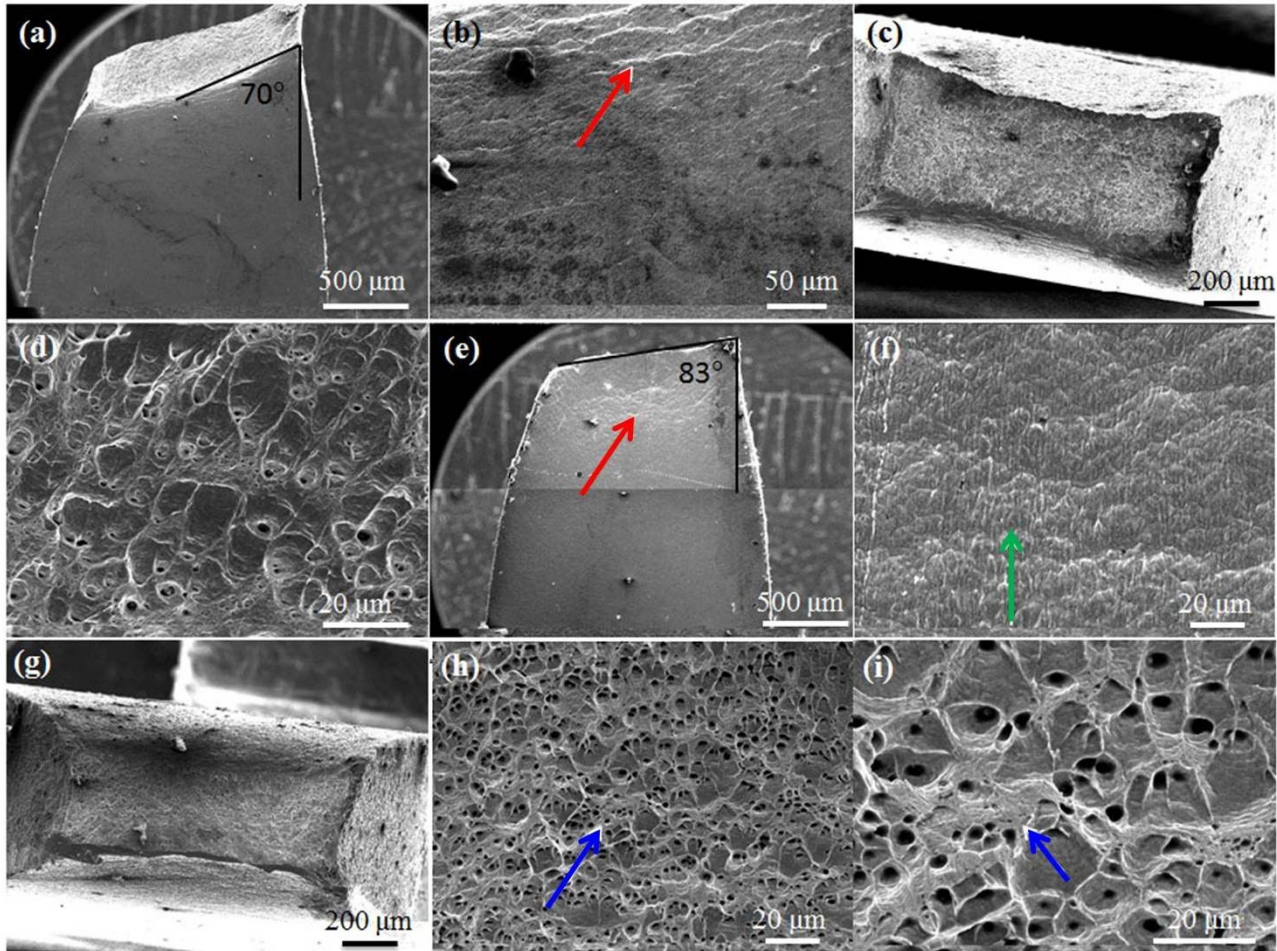
Figure 3: (a) The cross-section of as-ECAPed Cu after fracture; (b) the zoom-in view of location near necking part in Figure 3(a), deformed micro-bands parallel to fracture edge was pointed out by red arrow; (c) the fracture surface of as-ECAPed Cu; (d) the zoom-in view of location in Figure 3(c); (e) the cross-section of bimodal Cu after fracture, deformed micro-bands in horizontal direction were pointed by red arrow; (f) the zoom-in view of Figure 3(e), elongated recrystallized micro-grains in vertical direction were pointed out by green arrow; (g) the fracture surface of bimodal Cu; (h) the zoom-in view of Figure 3(g), small sub-micro-dimples formed from the UFG regions were pointed out by blue arrow; (i) the zoom-in view of Figure 3(h), small sub-micro-dimples formed from the UFG regions were pointed out by blue arrow.

consistent with the grain size distribution and suggests that the large micro-dimples were formed from the recrystallized regions, and the small sub-micro-dimples from the UFG regions.

To reveal the microstructural evolutions during tension, we further performed EBSD on the region near necking, as shown in Figure 4. Figure 4(a) is the orientation map of the annealed Cu sample after tensile test. On the right, the black zero-resolution pixels were affected by fracture. Elongated micro-grains were observed to parallel with tensile direction, the horizontal direction in Figure 4(a), and different from the bimodal Cu sample before tensile test. Figure 4(b) exhibits the local average misorientation map on Figure 4(a). The rainbow bar on top of Figure 4(b) is the same as in Figure 1(d). First of all, the overall fraction of non-blue areas rises to 44%, which implies the multi-

plication of deformation induced dislocation pile-ups and cells. Furthermore, the non-blue areas become increasingly dense approaching to the necking part. From left to right, deformation or stress is more focused as getting closer to necking, therefore the strain gradient is built by the deformation or stress induced difference of dislocation density. At last, the coincidence feature of blue areas/micro-grains and non-blue areas/UFGs becomes more distinctive as in less deformed areas. This feature manifests strain partition evolving with deformation in bimodal Cu. As in Figure 4(c), the pole figures of bimodal Cu are affected by tensile test and different from its counterpart in Figure 1(e). On one hand, {111} and {001} have the tendency to move toward the tensile direction. On the other hand, {001}, {110} and {111} also tend to rotate around the tensile direction.
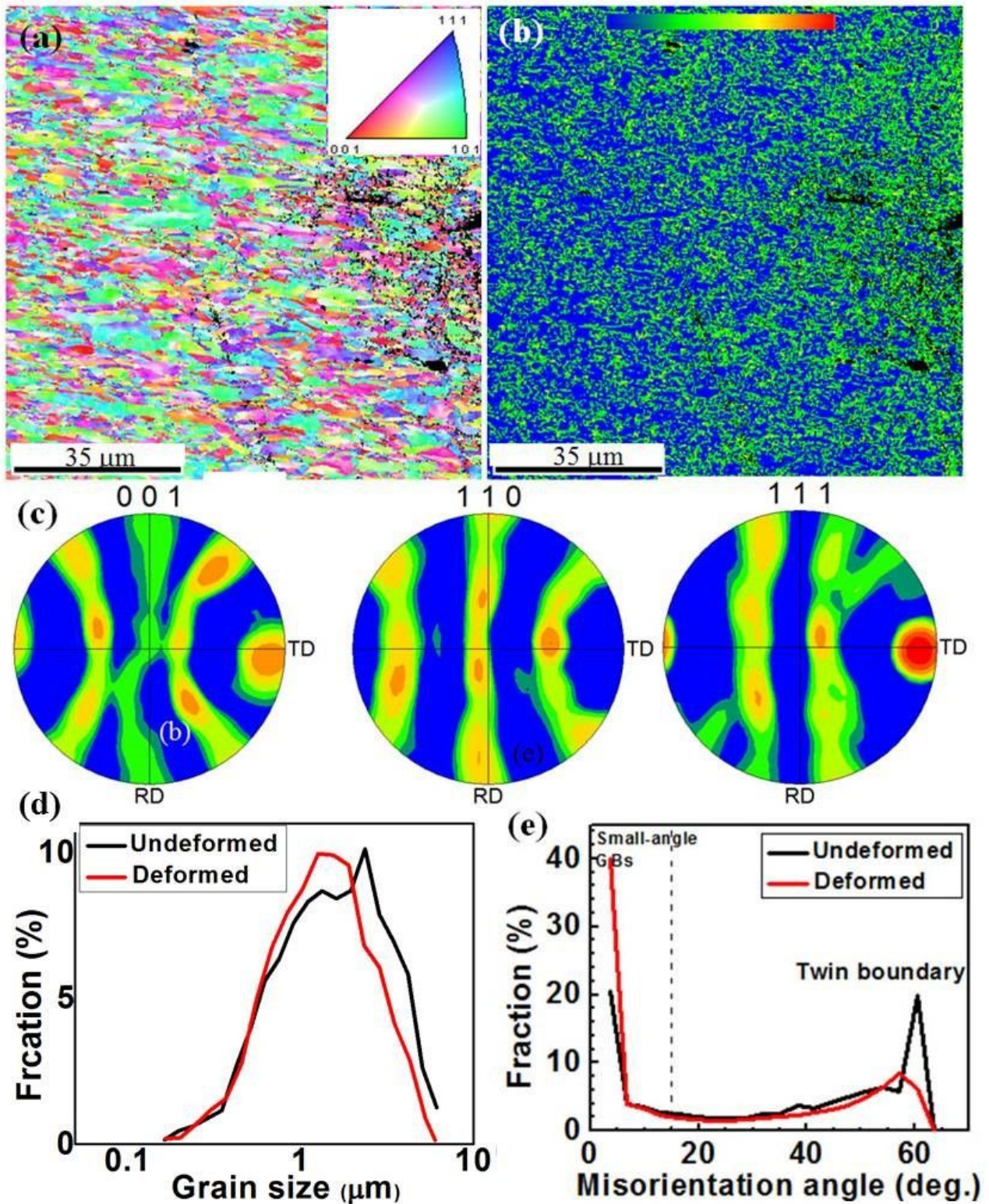
Figure 4: (a) The orientation mapping of bimodal Cu after tensile test; the inset is IPF-Z coloring code. (b) the local average misorientation map of Figure 4(a); (c) the pole figures of Figure 4(a); (d) the grain size distributions of bimodal Cu after and before tensile test; (e) the misorientation angle distributions of bimodal Cu after and before tensile test.

Figure 4(d) is the grain size distribution of bimodal Cu before (black line) and after (red line) tensile test. The red line shifts toward left to the black line, especially in the grain size range larger than 1 µm (*i.e.* the grain size of recrystallized micro-grains), and keeps nearly unchanged in the UFG region. These observations indicate that grain refinement occurred in micro-grains and the UFGs remain unchanged. During tensile deformation, the micro-grains burdened most of the strain and were severely deformed and elongated along the tensile axis. Dislocation activity including gliding, propagation, tangling and interaction plays a dominant role in the deformation of CGs because CGs provide adequate spacing for significant numbers of dislocation intersections during deformation. The UFGs retained more or less equiaxed shape (Figure 4a), so that the grain size measurement in Figure 4(e) is convincing.

Figure 4(e) plots the grain boundary misorientation angle distribution of bimodal Cu before (black line) and after (red line) tensile test. In the first place, the fraction of low angle (especially < 5°) grain boundary after tensile test is much larger than its counterpart. This phenomenon is related to dislocation multiplication and the formation of subgrain referred in Figure 4(b). Besides, at the 60° misorientation angle (denoting twins in cubic metals and alloys), the fraction decreases from 20% (before tensile test) to 6% (after tensile test). The reduction means detwinning happened in these micro-grains during tensile test.

4 Discussion

The EBSD analyses above indicate that grain refinement of recrystallized micro-grains occurred in annealed bimodal Cu sample during tension while the UFGs remained unchanged. In literature, *in situ* TEM investigations recorded two different grain growth mechanisms under deformation corresponding to two size regimes: the rotation and coalescence of grains with the size of 10 − 20 nm in the work by Shan *et al.* [35] and Wang *et al.* [36], and the GB migration for grains larger than 100 nm based on the results by Jin *et al.* [37] and Legros *et al.* [38]. These results imply that there is a grain size dependence of the mechanisms of deformation-induced grain growth. For the grain coarsening via grain rotation and grain coalescence, some models have been developed [36, 39]. With plastic deformation, grain boundary sliding occurs via gliding GB dislocations. A gliding GB dislocation splits at triple junction into two climbing GB dislocations, and the crystal lattice rotation in the neighboring grain will subsequently occur by these climbing GB dislocations (GB sliding transforms into ro-

tation of neighboring grain). This is also consistent with observations of MD simulations [40–42]. As for our bimodal Cu, we did not observe evident grain growth of the UFGs, although they were subjected to a large deformation strain. The coordinated deformation mechanisms underneath the UFGs and CGs propose a new scope for further investigations [43].

Using topological analysis and MD simulations, mechanisms of detwinning were elucidated in [44]. For twins in fcc lattices, either deformation or growth twins, their ends can be represented as incoherent twin boundaries (ITBs) formed by an array of Shockley partial dislocations [44–48]. As schematically shown in Figure 5(a), when a single twinning dislocation nucleates from the GB and glides inside the twin, two new stacking faults were formed inside the twin, and detwinning will not occur in this case. However, the twin becomes thinner with a magnitude of one (111) atomic plane thick, *i.e.* detwinning, when a single twinning dislocation nucleates from the GB and glides on the twin boundary, as shown in Figure 5(b). As shown in Figure 5(c), a detwinning process is accomplished through the collective glide of multiple twinning dislocations that form the ITBs. ITBs propagate as disconnections or steps with a height of multiple atomic planes. Therefore, the detwinning process occurs by migration of steps or disconnections
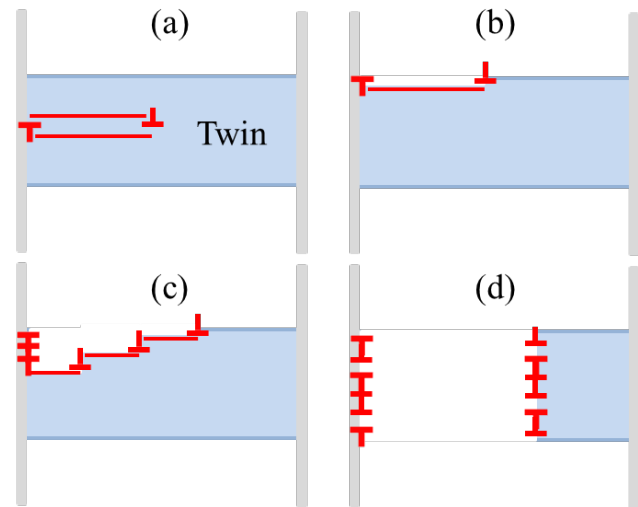
Figure 5: Schematic representation of detwinning process. GBs lie on both sides in all figures. The blue solid lines represent coherent twin boundaries, and the twin is marked in light blue. (a) A single twinning dislocation nucleates from the GB and glides inside the twin; (b) a single twinning dislocation nucleates from the GB and glides on the twin boundary; (c) multiple twin dislocations continuously nucleate from the GB and glide away on the twin boundary plane; (d) multiple twin dislocations with an arrangement of an ITB simultaneously nucleate at the GB, reorienting the originally twinned crystal into a matrix crystal through their gliding.

with step heights of the order of a few interplanar distances. This was also observed in the case of detwinning of growth twins in an electrodeposited nc Ni–Fe alloy during dynamic compression [49].

The detwinning process might specifically occur in growth twins of Cu with mediate stacking fault energy because under tensile stress state, the annealing growth twins are not stable and may reach new equilibrium state via detwinning. On the other hand, it is hard to introduce deformation twins in Cu via deformation at room tmperature and quasi-state deformation strain rate. This also hints that the annealing growth twins in Cu are not stable and try to find opportunity to detwin, as long as there is an activation, such as deformation.

5 Conclusions

In summary, a bimodal Cu with 80% volume fraction of recrystallized micro-grains was prepared by the annealing of as-ECAPed Cu at 473 K for 40 min. Mechanical properties was measured by tensile testing, and fracture and deformation mechanisms were measured by EBSD and SEM. Detailed results and conclusions are as following:

1. Compared with the as-ECAPed UFG Cu sample, which has a 0.2% yield strength of 370 MPa, an ultimate tensile strength of 410 MPa, an uniform elongation of 2% and an elongation to the failure of 16%, the bimodal Cu has an optimal strength-ductility combination (yield strength of 220 MPa and ductility of 34%).
2. Consistent with the high tensile ductility, the bimodal Cu has a larger shear fracture angle of 83° and a larger area reduction of 78% than the as-ECAPed UFG Cu sample, which has a shear fracture angle of 70° and an area reduction of 69%.
3. After tensile deformation, grain refinement of recrystallized micro-grains and detwinning of the annealing growth twins were observed in the necking part of the tensile specimen of the bimodal Cu. The underlying deformation mechanisms for grain refinement and detwinning were analyzed and discussed. It should be noted that the detwinning process might specifically occur in annealing growth twins because under tensile stress state, the annealing growth twins may reach new equilibrium state via detwinning.

Author contribution: Conceptualization, methodology, resources and material preparation, investigation and microstructural characterization, data curation, writing, supervision, project administration and funding acquisition, Y.H. Zhao; Discussion, Silu Liu; All authors have discussed and agreed to the published version of the manuscript.

Conflict of Interests: The authors declare that they have no known competing financial interests or personal relationships that could have appeared to influence the work reported in this paper.

Data availability statement: The data used to support the findings of this study are available from the corresponding author upon request.

References

[1] Morozova, A., R. Mishnev, A. Belyakov, R. Kaibyshev, Microstructure and properties of fine grained Cu-Cr-Zr alloys after thermo-mechanical treatments, Reviews on Advanced Materials Science, Vol. 54, No. 1, 2018, pp. 56-92.

[2] Ovid'ko, I. A., R. Z. Valiev, and Y. T. Zhu. Review on superior strength and enhanced ductility of metallic nanomaterials. Progress in Materials Science, Vol. 94, No. 2, 2018, pp. 462–540.

[3] Ni, H.T., J. Zhu, Z.D. Wang, H.Y. Lv, Y.Y. Su, X.Y. Zhang, A brief overview on grain growth of bulk electrodeposited nanocrystalline nickel and nickel-iorn alloys, Reviews on Advanced Materials Science, Vol. 58, No. 1, 2019, pp. 98-106.

[4] Koch, C. C., D. G. Morris, K. Lu, and A. Inoue. Ductility of nanostructured materials. MRS Bulletin, Vol. 24, No. 2, 1999, pp. 54–58.

[5] Bagheripoor M., R. Klassen, Length scale plasticity: A review from the perspective of dislocation nucleation, Reviews on Advanced Materials Science, Vol. 56, No. 1, 2018, pp. 21-61.

[6] Zhao, Y. H., J. F. Bingert, T. D. Topping, P. L. Sun, X. Z. Liao, Y. T. Zhu et al. Mechanical behavior, deformation mechanism and microstructure evolutions of ultrafine-grained Al during recovery via annealing. Materials Science and Engineering: A, Vol. 772, No. 138706, 2020, pp. 1-13.

[7] Orlova, T.S., A.M. Mavlyutov, T.A. Latynina, E.V. Ubyivovk, M.Y. Murashkin, R. Schneiders, D. Gerthsen, R.Z. Valiev, Influence of severe plastic deformation on microstructure, strength and electrical conductivity og aged Al-0.4Zr(wt%) alloy, Reviews on Advanced Materials Science, Vol. 58, No. 1-2, 2018, pp. 92-101.

[8] Megumi, K., T.G. Langdon, Superplasticity in ultrafine-grained materials, Reviews on Advanced Materials Science, Vol. 54, No. 1, 2018, pp.46-55.

[9] Zhao, Y. H., Y. T. Zhu, and E. J. Lavernia. Strategies for improving tensile ductility of bulk nanostructured materials. Advanced Engineering Materials, Vol. 12, No. 8, 2010, pp. 769–778.

[10] Legros, M., B. R. Elliott, M. N. Rittner, J. R. Weertman, and K. J. Hemker. Microsample tensile testing of nanocrystalline metals. Philosophical Magazine A, Vol. 80, No. 4, 2000, pp. 1017–1026.

[11] Tellkamp, V. L., E. J. Lavernia, and A. Melmed. Mechanical behavior and microstructure of a thermally stable bulk nanostructured Al alloy. Metallurgical and Materials Transactions A, Vol. 32, No. 9, 2001, pp. 2335–2343.

[12] Wang, Y. M., M. Chen, F. Zhou, and E. Ma. High tensile ductility in a nanostructured metal. Nature, Vol. 419, No. 6910, 2002, pp. 912–915.

[13] Zhao, Y. H., T. Topping, J. F. Bingert, J. J. Thornton, A. M. Dangelewicz, Y. Li et al. High tensile ductility and strength in bulk nanostructured nickel. Advanced Materials, Vol. 20, No. 16, 2008, pp. 3028–3033.

[14] Zhao, Y. H., and E. J. Lavernia. The mechanical properties of multiscale metallic materials. In Nanostructured Metals and Alloys, Whang, S. H., Elsevier, 2011, pp. 375–429.

[15] Billard, S., J. P. Fondère, B. Bacroix, and G. F. Dirras. Macroscopic and microscopic aspects of the deformation and fracture mechanisms of ultrafine-grained aluminum processed by hot isostatic pressing. Acta Materialia, Vol. 54, No. 2, 2006, pp. 411–421.

[16] Jin, H., and D. J. Lloyd. Effect of a duplex grain size on the tensile ductility of an ultra-fine grained Al–Mg alloy, AA5754, produced by asymmetric rolling and annealing. Scripta Materialia, Vol. 50, No. 10, 2004, pp. 1319–1323.

[17] Tang, F., M. Hagiwara, and J. Schoenung. Formation of coarse-grained inter-particle regions during hot isostatic pressing of nanocrystalline powder. Scripta Materialia, Vol. 53, No. 6, 2005, pp. 619–624.

[18] Fan, G. J., H. Choo, P. K. Liaw, and E. J. Lavernia. Plastic deformation and fracture of ultrafine-grained Al–Mg alloys with a bimodal grain size distribution. Acta Materialia, Vol. 54, No. 7, 2006, pp. 1759–1766.

[19] Srinivasarao, B., K. Oh-ishi, T. Ohkubo, T. Mukai, and K. Hono. Synthesis of high-strength bimodally grained iron by mechanical alloying and spark plasma sintering. Scripta Materialia, Vol. 58, No. 9, 2008, pp. 759–762.

[20] Zhao, M. C., F. Yin, T. Hanamura, K. Nagai, and A. Atrens. Relationship between yield strength and grain size for a bimodal structural ultrafine-grained ferrite/cementite steel. Scripta Materialia, Vol. 57, No. 9, 2007, pp. 857–860.

[21] Azizi-Alizamini, H., M. Militzer, and W. J. Poole. A novel technique for developing bimodal grain size distributions in low carbon steels. Scripta Materialia, Vol. 57, No. 12, 2007, pp. 1065–1068.

[22] Niendorf, T., D. Canadinc, H. Maier, and I. Karaman. The role of grain size and distribution on the cyclic stability of titanium. Scripta Materialia, Vol. 60, No. 5, 2009, pp. 344–347.

[23] Lee, Z., V. Radmilovic, B. Ahn, E. J. Lavernia, and S. R. Nutt. Tensile deformation and fracture mechanism of bulk bimodal ultrafine-grained Al-Mg alloy. Metallurgical and Materials Transactions A, Vol. 41, No. 4, 2009, pp. 795–801.

[24] Wu, X. L., M. X. Yang, F. Yuan, G. Wu, Y. Wei, X. X. Huang et al. Heterogeneous lamella structure unites ultrafine-grain strength with coarse-grain ductility. Proceedings of the National Academy of Sciences, Vol. 112, No. 47, 2015, pp. 14501–14505.

[25] Zhu, Y. T., and X. L. Wu. Perspective on hetero-deformation induced (HDI) hardening and back stress. Materials Research Letters, Vol. 7, No. 10, 2019, pp. 393–398.

[26] Huang, C. X., Y. F. Wang, X. L. Ma, S. Yin, H. W. Höppel, M. Göken et al. Interface affected zone for optimal strength and ductility in heterogeneous laminate. Materials Today, Vol. 21, No. 7, 2018, pp. 713–719.

[27] Gao, H. J. Mechanism-based strain gradient plasticity? I. Theory. Journal of the Mechanics and Physics of Solids, Vol. 47, No. 6, 1999, pp. 1239–1263.

[28] Liu Y. F., Y. Cao, Q. Z. Mao, H. Zhou, Y. H. Zhao, W. Jiang et al. Critical microstructures and defects in heterostructured materials and their effects on mechanical properties. Acta Materialia, Vol. 189, No. 1, 2020, pp. 129-144.

[29] Zhao, Y. H., T. Topping, Y. Li, and E. J. Lavernia. Strength and ductility of bi-modal Cu. Advanced Engineering Materials, Vol. 13, No. 9, 2011, pp. 865–871.

[30] Zhao, Y.H., Y. Li, T.D. Topping, X.Z. Liao, Y.T. Zhu, R.Z. Valiev, E.J. Lavernia, Ductility of ultrafine-grained copper processed by equal-channel angular pressing, Int. J. Mater.Res. (former: Z. Metallkd), vol. 100, No. 2009, pp. 1647-1652.

[31] Valiev, R. Z., R. Islamgaliev, and I. Alexandrov. Bulk nanostructured materials from severe plastic deformation. Progress in Materials Science, Vol. 45, No. 2, 2000, pp. 103–189.

[32] Beyerlein, I. J., and L. S. Tóth. Texture evolution in equal-channel angular extrusion. Progress in Materials Science, Vol. 54, No. 4, 2009, pp. 427–510.

[33] Li, S., I. J. Beyerlein, D. J. Alexander, and S. C. Vogel. Texture evolution during multi-pass equal channel angular extrusion of copper: Neutron Diffraction Characterization and Polycrystal Modeling. Acta Materialia, Vol. 53, No. 7, 2005, pp. 2111–2125.

[34] Zhang, Z. F., and J. Eckert. Unified tensile fracture criterion. Physical Review Letters, Vol. 94, No. 9, 2005, pp. 094301.1-094301.4.

[35] Shan, Z. W., E. A. Stach, J. M. K. Wiezorek, J. A. Knapp, D. M. Follstaedt, and S. X. Mao. Grain boundary-mediated plasticity in nanocrystalline nickel. Science, Vol. 305, No. 5684, 2004, pp. 654–657.

[36] Wang, Y. B., B. Q. Li, M. L. Sui, and S. X. Mao. Deformation-induced grain rotation and growth in nanocrystalline Ni. Applied Physics Letters, Vol. 92, No. 1, 2008, pp. 11903.1-11903.4.

[37] Gutkin, M. Y., I. A. Ovid'ko, and N. V. Skiba. Crossover from grain boundary sliding to rotational deformation in nanocrystalline materials. Acta Materialia, Vol. 51, No. 14, 2003, pp. 4059–4071.

[38] Haslam, A., S. Phillpot, D. Wolf, D. Moldovan, and H. Gleiter. Mechanisms of grain growth in nanocrystalline fcc metals by molecular-dynamics simulation. Materials Science and Engineering: A, Vol. 318, No. 1–2, 2001, pp. 293–312.

[39] Haslam, A. J., D. Moldovan, V. Yamakov, D. Wolf, S. R. Phillpot, and H. Gleiter. Stress-enhanced grain growth in a nanocrystalline material by molecular-dynamics simulation. Acta Materialia, Vol. 51, No. 7, 2003, pp. 2097–2112.

[40] Jin, M., A. M. Minor, E. A. Stach, and J. W. Morris. Direct observation of deformation-induced grain growth during the nanoindentation of ultrafine-grained Al at room temperature. Acta Materialia, Vol. 52, No. 18, 2004, pp. 5381–5387.

[41] Legros, M., D. S. Gianola, and K. J. Hemker. In situ TEM observations of fast grain-boundary motion in stressed nanocrystalline aluminum films. Acta Materialia, Vol. 56, No. 14, 2008, pp. 3380–3393.

[42] Moldovan, D., D. Wolf, and S. R. Phillpot. Theory of diffusion-accommodated grain rotation in columnar polycrystalline microstructures. Acta Materialia, Vol. 49, No. 17, 2001, pp. 3521–3532.

[43] Liu S., Y. Wang, Y.H. Zhao, Revealing plastic deformation mechanisms of grain rotation in a heterogeneous bimodal Cu, sumitted

to Internal Journal of Plasticity.

[44] Wang, J., N. Li, O. Anderoglu, X. Zhang, A. Misra, J. Y. Huang *et al*. Detwinning mechanisms for growth twins in face-centered cubic metals. Acta Materialia, Vol. 58, No. 6, 2010, pp. 2262–2270.

[45] Wang, J., O. Anderoglu, J. P. Hirth, A. Misra, and X. Zhang. Dislocation structures of Σ3 {112} twin boundaries in face centered cubic Metals. Applied Physics Letters, Vol. 95, No. 2, 2009, pp. 21908.1-21908.4.

[46] Hu, Q., L. Li, and N. M. Ghoniem. Stick–slip dynamics of coherent twin boundaries in copper. Acta Materialia, Vol. 57, No. 16, 2009, pp. 4866–4873.

[47] Gao X. Z., L. J. Dai, and Y. H. Zhao. Twin boundary-dislocation interactions in nanocrystalline Cu-30% Zn alloys prepared by high pressure torsion. Journal of Materials Research and Technology, Vol. 9, No. 5, 2020, pp. 11958-11967.

[48] Li, Y. S., L. J. Dai, Y. Cao, Y. H. Zhao, and Y. T. Zhu. Grain size effect on deformation twin thickness in a nanocrystalline metal with low stacking-fault energy. Journal of Materials Research, Vol. 34, No. 13, 2019, pp. 2398-2405.

[49] Cheng, S., Y. H. Zhao, Y. Z. Guo, Y. Li, Q. M. Wei, X. L. Wang *et al*. High plasticity and substantial deformation in nanocrystalline NiFe alloys under dynamic loading. Advanced Materials, Vol. 21, No. 48, 2009, pp. 5001–5004.